

1D SnO₂ with Wire-in-Tube Architectures for Highly Selective Electrochemical Reduction of CO₂ to C₁ Products

Lei Fan, Zheng Xia, Meijia Xu, Yingying Lu,* and Zhongjian Li*

Electrochemical reduction of CO₂ (ERC) into useful products, such as formic acid and carbon monoxide, is a fascinating approach for CO₂ fixation as well as energy storage. Sn-based materials are attractive catalysts for highly selective ERC into C₁ products (including HCOOH and CO), but still suffer from high overpotential, low current density, and poor stability. Here, One-dimensional (1D) SnO₂ with wire-in-tube (WIT) structure is synthesized and shows superior selectivity for C₁ products. Using the WIT SnO₂ as the ERC catalyst, very high Faradaic efficiency of C₁ products (>90%) can be achieved at a wide potential range from -0.89 to -1.29 V versus RHE, thus substantially suppressing the hydrogen evolution reaction. The electrocatalyst also exhibits excellent long-term stability. The improved catalytic activity of the WIT SnO₂ over the commercial SnO₂ nanoparticle indicates that higher surface area and large number of grain boundaries can effectively enhance the ERC activity. Synthesized via a facile and low-cost electrospinning technology, the reduced WIT SnO₂ can serve as a promising electrocatalyst for efficient CO₂ to C₁ products conversion.

transformation route with high application prospect, due to its environmental-friendly nature and compatibility with other renewable energy sources such as wind turbines and solar panels.^[5-7]

Formic acid is a high-value added and energy dense chemical feedstock, which is commonly used in various industries.^[8,9] CO is also one of the desired products from the reduction of CO₂, because CO, a platform chemical, can be further reduced to oxygenates and hydrocarbons electrochemically.^[10] Therefore, HCOOH and CO are two main C₁ products of ERC. In previously studies, noble metal-based electrocatalysts for ERC have shown favorable results to generate C₁ products (CO and HCOOH) at a low overpotential. However, their implementation at an industrial scale is unsustainable and not economically feasible owing to the scarcity of noble

1. Introduction

The concentration of CO₂ in the atmosphere has been increased from 278 to >400 ppm since the industrial revolution, and this phenomenon has been recognized as the primary culprit for global warming, which results in desertification, deglaciation, and the arise of the mean sea level.^[1-4] Electrochemical reduction of CO₂ (ERC) to energy products is an important

metals.^[11-13] Besides noble metals, various non-noble materials have been used as heterogeneous electrocatalysts to reduce CO₂ to CO or HCOOH, including transition metals (e.g., Cu,^[14] Pb,^[15] and In^[16,17]), transition-metal oxides (e.g., Co₃O₄,^[18] TiO₂,^[19] and SnO₂^[20,21]), transition-metal dichalcogenides (e.g., MoS₂,^[22] WSe₂,^[23] and SnS₂^[24]), and carbon-based materials (e.g., carbon nanotubes^[25] and carbon nanofibers^[26]). Among all these catalysts, an attractive alternative for noble metal electrodes is the use of tin and its dioxide. However, poor activity, selectivity, and stability in the formation of CO and formic acid impeded the practical application of polycrystalline tin. Various approaches have been proposed to solve these problems. Sn/SnO_x composite thin-film catalyst has been used to stabilize the *CO₂⁻ intermediate and enhance the reduction activity.^[20] 3D hierarchical SnO₂ electrodes have also been fabricated to promote the charge and mass transfer during ERC.^[7] Structural defects such as grain boundaries (GBs) can further enhance the active sites for electrochemical reaction. Kumar et al. reported that the SnO₂ porous nanowires with a high density of GBs can improve CO₂ reduction performance toward HCOOH.^[27] This improvement in HCOOH Faradaic efficiency (FE) (~80%) is attributed to the broken local spatial symmetry near the GBs that tuned the binding energy of the reaction intermediate. These results indicate that the electrocatalytic activity is highly dependent on the morphology, chemical composition, and amount of catalytically active sites. Therefore, developing an Sn-based catalyst that provides unique nanostructure and abundant active sites can lead to an improved FE for CO₂ reduction to C₁ products.

L. Fan, Z. Xia, Prof. Y. Lu, Prof. Z. Li
College of Chemical and Biological Engineering
Zhejiang University
Hangzhou 310027, China
E-mail: yingyinglu@zju.edu.cn; zdlizj@zju.edu.cn

L. Fan, Prof. Y. Lu
State Key Laboratory of Chemical Engineering
Institute of Pharmaceutical Engineering
Zhejiang University
Hangzhou 310027, China

M. Xu
Department of Chemistry
Zhejiang University
Hangzhou 310027, China

Prof. Z. Li
Key Laboratory of Biomass Chemical Engineering of Ministry
of Education
Zhejiang University
Hangzhou 310027, China

 The ORCID identification number(s) for the author(s) of this article can be found under <https://doi.org/10.1002/adfm.201706289>.

DOI: 10.1002/adfm.201706289

One-dimensional (1D) materials have long been applied in energy storage and conversion, such as lithium-based batteries,^[28] supercapacitors,^[29] and hydrogen evolution reactions (HERs).^[30] When used as electrocatalysts, the 1D structure owns higher surface area and thus provides more active sites.^[29] Furthermore, 1D structure can also facilitate the charge transfer at the electrode/electrolyte interfaces due to the enhanced contact with electrolyte. Besides, compared with bulk materials, low-dimensional nanostructure materials can enhance the structure stability and mechanical stability during electrochemical reactions.^[29] However, very little attention has been paid to the development of 1D nanostructure materials to improve the ERC performance.

Motivated by the above consideration, a novel 1D wire-in-tube (WIT) structured SnO₂ nanofiber was fabricated by electrospinning and calcining. Specifically, a pristine electrospun nanofiber is transformed into a WIT structure nanofiber after oxidizing at atmosphere. Compared with commercial SnO₂ nanoparticles, the 1D WIT SnO₂ nanofiber evolves a higher density of GBs during the calcining process. The special atomic structure and favorable electron transport of GBs can be used to stabilize the active surfaces of the electrocatalysts. Therefore, the WIT SnO₂ can transform CO₂ into C₁ products including HCOOH and CO selectively and efficiently.

2. Results and Discussion

2.1. Synthesis of the WIT SnO₂ Nanofiber

Reduced SnO₂ has shown to be an effective electrochemical catalyst to transform CO₂ to formate with high selectivity, due to its intrinsic active sites for ERC. By tuning the morphology and crystalline structure, the selectivity and catalysis activity of SnO₂ can be further improved. The WIT SnO₂ nanofiber was synthesized by electrospinning. The fabrication process and formation mechanism of the WIT SnO₂ nanofiber were illustrated in **Figure 1a**. The pristine electrospun nanofiber is

composed of SnCl₂·2H₂O and poly(vinylpyrrolidone) (PVP) with mixed solvent, *N,N*-dimethylformamide (DMF) with ethyl alcohol (EtOH), 1:1 by volume). The WIT structure was obtained through calcination with the following speculated mechanism: At the beginning of the calcination process, low boiling point EtOH (boiling point of EtOH = 78 °C) in the pristine electrospun nanofibers evaporates first. Since SnCl₂·2H₂O has higher solubility in EtOH than in the PVP dissolved DMF, metal precursor tends to be attracted to the outer parts of the nanofiber and form an outer shell during the initially calcination step.^[31] As temperature elevated, DMF (boiling point of DMF = 152 °C) begins to evaporate. The inner PVP assists the Ostwald ripening of the remained metal precursor in the gel matrix and the diffusion of gas-phase EtOH and DMF generates an outward force.^[32] Meanwhile, the viscoelastic PVP begins to contract and thus arise another inward force. By balancing these two forces, the outer shell and the gel matrix are split at a certain point.^[33] Finally, both gel matrix and metal precursor decompose and form the crystallized WIT SnO₂ nanofiber. The crystal structures of the WIT SnO₂ nanofibers (Figure S2a, Supporting Information) and commercial SnO₂ nanoparticles (NP SnO₂, Figure S2b, Supporting Information) were characterized by X-ray diffraction (XRD), which can be indexed to the rutile tetragonal phase SnO₂ (JCPDS card No. 41–1445). The diffraction lines of both catalysts are nearly indistinguishable, which demonstrates a high similarity in crystallinity of the WIT SnO₂ nanofiber and NP SnO₂. Also, the almost identical diffraction peaks suggest that the synthesized WIT SnO₂ nanofiber involves negligible impurities to SnO₂.

The surface morphology of the synthesized nanofibers was characterized by scanning electron microscopy (SEM). The diameter of the pristine nanofiber ranges from 350 to 500 nm, and the length is each nanofiber is about tens of micrometers (Figure S3, Supporting Information). After oxidation, both the length and the diameter have no obvious change (Figure 1b–d). Nonetheless, the solid nanofiber turns into a complex construction, which constitutes of a hollow tube and a solid wire with a

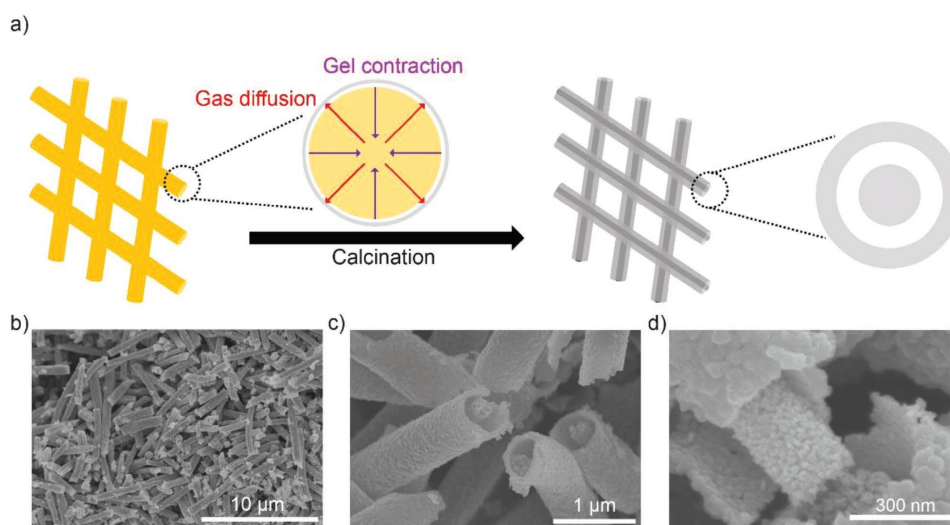


Figure 1. Schematic representation of the synthesis process and mechanism of a) the WIT SnO₂ nanofibers and b–d) SEM images of the WIT SnO₂ nanofibers at various magnifications.

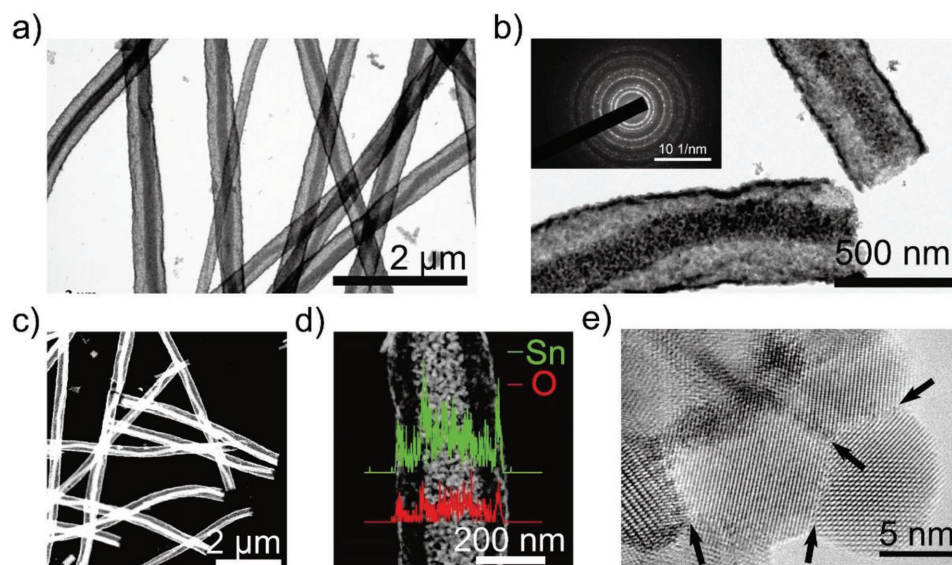


Figure 2. Characteristics of the WIT SnO₂ nanofibers. a,b) HRTEM images of the WIT SnO₂ nanofibers. The inset in panel (b) is SAED pattern of the SnO₂ nanofibers. c,d) Scanning TEM images of the WIT SnO₂ nanofibers. The inset in panel (d) is the line scan results, which show the distributions of Sn and O elements. e) Magnified TEM image of the WIT SnO₂ nanofibers with a high density of GBs.

diameter of 150–250 nm. As explained previously, the formation mechanism is based on the interactions between the metal precursor, gel matrix, and solvent in the calcination process.

High-resolution transmission electron microscopy (HRTEM) is employed to further determine the structure of the WIT SnO₂ nanofibers. As shown in **Figure 2a,b**, the observed structure is consistent with the SEM results. The selected-area electron diffraction (SAED) pattern (inset of **Figure 2b**) suggests the poly-

crystalline nature of the SnO₂ nanofibers. The WIT structure is more distinct when observed by scanning TEM (**Figure 2c,d**). Interestingly, the inside wire is composed of SnO₂ nanoparticles with nanoporous structure (**Figure 2d**). Line scan results inserted in **Figure 2d** show the stannum (Sn) and oxygen (O) elemental distributions of the cross-section of the nanofiber. The middle of the nanofiber has higher Sn and O content, which indicates the existence of an interior nanowire. Detailed TEM image shown in **Figure 2e** suggests that the nanofiber is composed of nanoparticles with a diameter of about 10–20 nm. Nanoparticles are interconnected through GBs, which is visible in detailed HRTEM image. In the scale of 20 nm, the WIT SnO₂ approximately had about 4–8 GBs (indicated by arrows in **Figure 2e**). The projected GB length was about 5–10 nm. By contrast, bare SnO₂ nanoparticles appear as an aggregation of overlapping particles without GBs (**Figure S4**, Supporting Information). Recent publications have proposed that GBs can improve the ERC activity due to their favorable electrochemical properties.^[26,34–36]

Nitrogen adsorption–desorption isotherms were conducted to determine the Brunauer–Emmett–Teller (BET) surface area and porosity of the WIT SnO₂ nanofibers and the NP SnO₂. They display a type IV isotherm, with the WIT SnO₂ nanofibers to be more microporous and (**Figure 3a**). The average pore size of the WIT SnO₂ fiber is about 15 nm (**Figure 3b**). The BET surface area of the WIT SnO₂ nanofiber and the NP SnO₂ are 30.0 and 4.6 m² g⁻¹, respectively. The higher surface area, which is attributed to the WIT structure and the porous inner wire, enables more active sites and eventually improves the catalysis activity for ERC.

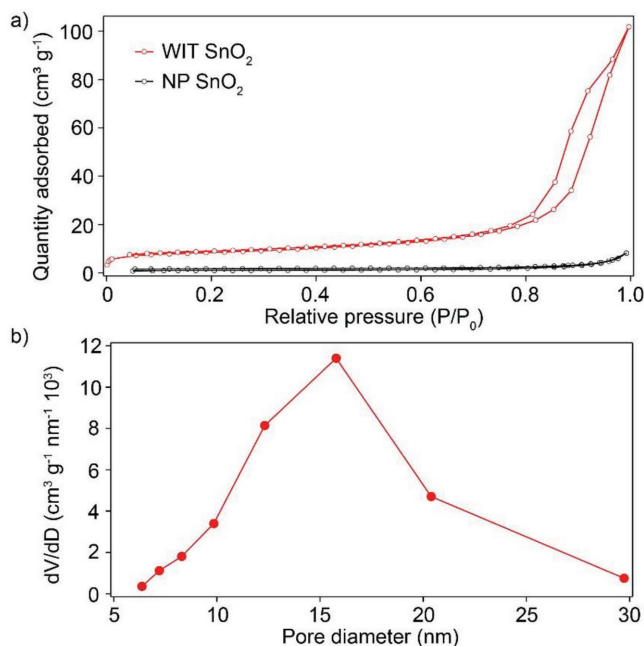


Figure 3. a) Nitrogen adsorption–desorption isotherms at 77 K of the WIT SnO₂ nanofibers (red) and the NP SnO₂ (black). b) Pore size distributions of the WIT SnO₂ nanofibers.

2.2. Electrochemical CO₂ Reduction Performance Evaluations

To evaluate the ERC performance of the WIT SnO₂, linear sweep voltammetry (LSV) of the WIT SnO₂ electrode in N₂

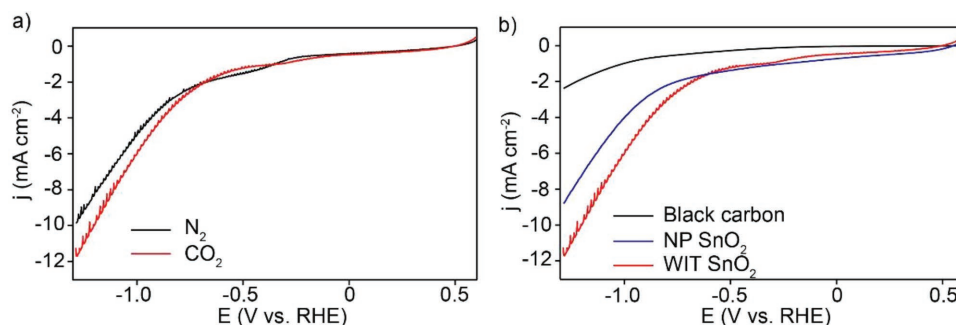


Figure 4. LSVs of the WIT SnO₂ electrode at a) N₂/CO₂ saturated solution and b) LSVs of the NP SnO₂, blank carbon paper and the WIT SnO₂ electrode in CO₂ saturated KHCO₃.

and CO₂ saturated 0.1 M KHCO₃ solution was conducted. The LSV curves in **Figure 4a** illustrates that the WIT SnO₂ delivers around 10 mA cm⁻² current density at -1.29 V in N₂-saturated solution with only the HER. Notably, a cathodic peak was observed at -0.4 V, which is corresponding to SnO₂ reduction to Sn²⁺ when scanning to negative potentials.^[13,37] This suggests that reduction of SnO₂ is likely prior to the ERC. In CO₂-saturated electrolyte, a current density of about 12 mA cm⁻², significantly higher than that in N₂ saturated electrolyte, was observed at -1.29 V. This current increasing indicates that the WIT SnO₂ nanofiber has an obvious catalytic activity on the ERC. However, as previously reported, the electrolyte pH shift between the N₂-saturated electrolyte and the CO₂-saturated electrolyte has to be taken into account (pH = 8.2 for N₂-saturated electrolyte versus pH = 6.8 for CO₂-saturated electrolyte). To involve the effect of the pH shift, LSVs are also plotted in an RHE scale. But in RHE scale, the potential-current behavior in both electrolytes has almost no difference. Therefore, further evidences are needed to confirm the ERC catalytic performance for the WIT SnO₂ electrode. Along this line, an NP SnO₂ electrode and a blank carbon paper were chosen as two comparisons and their LSVs were also measured in CO₂-saturated electrolyte. As shown in **Figure 4b**, for the WIT SnO₂ electrode, the onset potential appears at -0.69 V and the reductive current density reaches 7.6 mA cm⁻² at -1.09 V. For the NP SnO₂ electrode, a large reductive current appears at -0.99 V and reaches a current density of 5.2 mA cm⁻² at -1.09 V. The current density of the NP SnO₂ catalyst is lower than that of the WIT SnO₂ electrode at all potentials. The blank carbon paper without any catalyst showed a negligible current density, only 1.3 mA cm⁻² was obtained at -1.09 V. The LSVs illustrate that the current density of the WIT SnO₂ electrode is about 1.4 times of the NP SnO₂ electrode and five times of the black carbon at -1.09 V. Furthermore, the WIT SnO₂ electrode has a more positive onset potential about -0.59 V indicating the corresponding overpotential for the catalyst is only about 400 mV, which suggests that the WIT SnO₂ electrodes enable the ERC with a lower overpotential than the NP SnO₂ electrode. These results demonstrate that the WIT SnO₂ catalyst has a better catalytic activity on the ERC than the NP SnO₂. Because the current density was obtained based on the same catalyst mass loading per geometrical surface area on the WIT SnO₂ electrode and the NP SnO₂ electrode, the large surface area of the WIT

SnO₂ electrode might be an important factor leading to the enhancement of the ERC performance.

The ERC performance of the WIT SnO₂ electrode was further evaluated in constant potential electrolysis. **Figure S5** of the Supporting Information shows the electrolysis current density during the ERC for the WIT SnO₂ electrode at different electrolysis potentials. The electrolysis current density has a strong positive correlation with potentials, consistent with the result of LSV (**Figure S5a**, Supporting Information). In addition, the electrolysis current density versus time was also recorded for the WIT SnO₂ electrode at all potentials (**Figure S5b**, Supporting Information). H₂ and CO are the major gaseous products and HCOOH is the only liquid product can be detected. **Figure 5** shows the FEs of C₁ products (**Figure 5a**), HCOOH (**Figure 5b**), CO (**Figure 5c**), and H₂ (**Figure 5d**) of the WIT SnO₂ and NP SnO₂ electrodes as a function of potentials. The products distribution is found to be dependent on the applied potential. The maximized FE of CO is 36% at the applied potential of -0.89 V. HCOOH was detected as the main product (FE > 50%) at -0.89 V and the FEs are higher at more negative potentials. The HCOOH FE of the WIT SnO₂ electrode is higher than that of the NP SnO₂ electrode at all potentials. Specifically, at -0.89 V, the FE for HCOOH attains a value of 53% on the WIT SnO₂ electrode. While only 30% is achieved for the NP SnO₂ electrode. As well known, SnO₂ is few catalysts that convert CO₂ to HCOOH and CO with high selectivity. HCOOH and CO are both very widely used products in industry. Formic acid is a high-value added energy chemical used as fuel in formic acid fuel cells as well as a hydrogen storage material. CO is an important platform chemical in industries. Also, separation CO from HCOOH is easy, based on their different solubility in water. From this aspect, instead of focusing on improving FEs of one particular product (CO or HCOOH), C₁ products selectivity is a better index for evaluating the catalysts performance in this study. At -0.99 V, the FE of HCOOH reaches a maximum of 63% and the CO production reaches an FE of 30%. Meanwhile, the FE of hydrogen is suppressed to less than 5%. The total FE for C₁ products is as high as 93% showing an excellent C₁ products selectivity and HER suppression for the WIT SnO₂ electrode. Additionally, the high C₁ products selectivity of the WIT SnO₂ electrode can be achieved in a very wide potential range. With a potential ranging from -0.89 to -1.29 V, FEs for C₁ products on the WIT SnO₂ are consistently above 90% and FEs for HER are suppressed below 10%. While for

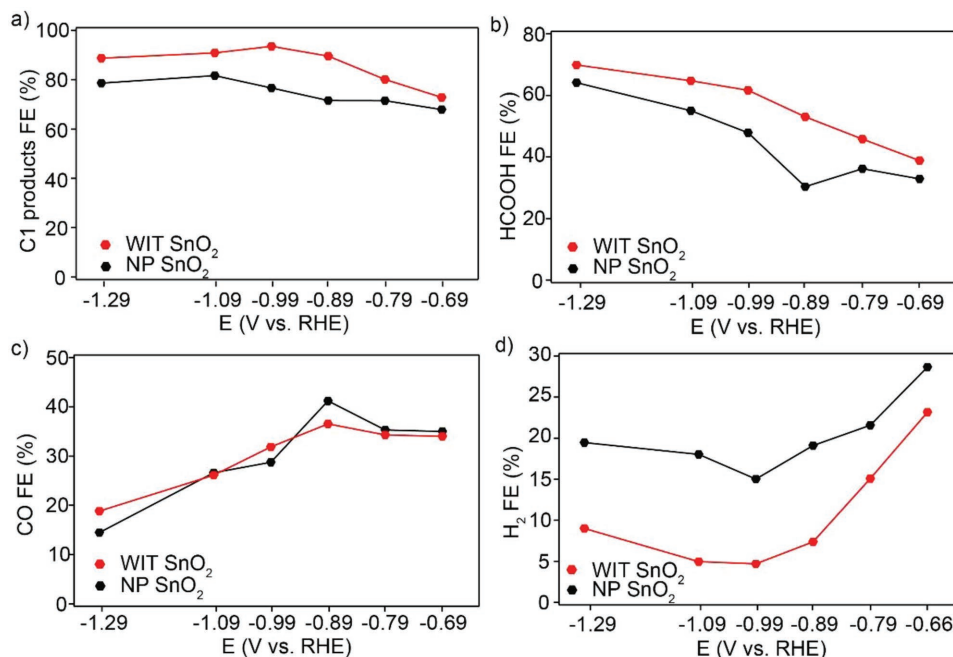


Figure 5. FE of a) C₁ products, d) HCOOH, c) CO, and d) H₂ for the WIT SnO₂ electrode and the NP SnO₂ electrode.

the NP SnO₂ electrode, the minimum HER FE is 15%, much higher than that of the WIT SnO₂ electrode. Since all tested electrodes were fabricated on carbon paper substrate, a control experiment was conducted to exclude the catalytic performance of the blank carbon paper. FEs of H₂ above 80% were observed with blank carbon paper electrode at all potentials (Figure S6, Supporting Information), which confirms that the C₁ products conversion is exclusively due to the WIT SnO₂ nanofiber. To summarize, the WIT SnO₂ catalyst exhibits efficient ERC performance by significantly improving the ERC selectivity toward C₁ products compared to the NP SnO₂. Different state-of-the-art Sn-based catalysts for C₁ products FE have been compared in Table S1 of the Supporting Information, which further illustrate the excellent ERC performance of the WIT SnO₂ nanofiber.

A long-term electrolysis for the WIT SnO₂ catalyst was carried out to investigate the catalyst stability. The gaseous products distribution was examined with respect to time at -0.69 V (Figure S7, Supporting Information). Concentration of the gaseous products was measured at 30 min intervals while the liquid product HCOOH FE was calculated at the end of the experiments. A current density of -2 mA cm⁻² and an FE of CO of 30% were maintained for 14 h, while the FE of H₂ was about 20% during the entire test. The NMR results indicate that the overall FE of HCOOH during the entire time period is 37%. Neither the current density nor the FEs of CO and H₂ are influenced with time. Furthermore, we observed that the WIT structure and GBs were retained after 14 h electrochemical reduction (Figure 6a,b). These results prove that the WIT SnO₂ electrode has an excellent electrostability.

X-ray photoelectron spectrometer (XPS) was employed to compare the composition and the stannic bonding modes of catalysts before and after electrolysis. The existence of an SnO₂ surface layer on the WIT SnO₂ catalyst before electrolysis is confirmed by the XPS results. As shown in Figure 6c, the doublet

peaks of the unused WIT SnO₂ sample at 495.5 and 487.0 eV correspond to the typical Sn 3d^{3/2} and Sn 3d^{5/2} peaks in SnO₂ (Sn⁴⁺). The prepared WIT SnO₂ nanofiber shows only twin SnO₂ peaks without any Sn core on electrode surface. After electrolysis, the Sn 3d signals are shifted to lower binding energy at 494.3 and 486.0 eV, which is assigned to SnO (Figure 6d).^[13,37] This transformation implies that the tin oxide surface layer is reduced during the electrolysis.

2.3. Discussions

According to the results presented above, significant enhancement for C₁ products selectivity and current density in the ERC was observed for the WIT SnO₂ catalyst over the NP SnO₂ catalyst. The HER is substantially suppressed on the WIT SnO₂ catalyst and high C₁ products selectivity is obtained. A straightforward hypothesis for the enhancement is higher catalyst surface area of the WIT SnO₂. Surface area of these two catalysts was measured using BET analysis. The results indicate that the surface area of the WIT SnO₂ is around ten times of that of NP SnO₂. This high surface area might introduce more active surface sites for *CO₂⁻ absorption. By contrast, the current density of the WIT SnO₂ electrode at -1.09 V is only about 1.4 times of the NP SnO₂ electrode. The increase of chronoamperometric current density is not directly proportional to surface area difference. This is because mass transport limitation on the WIT SnO₂ electrode (including reactants and intermediates) allows only a small portion of active sites on surface to participate in the ERC. More importantly, according to Gouy–Chapman theory, electrical double layer (EDL) could have a major effect on the electrochemical reactions. EDL will overlap the electric field easily in nanoporous structures thereby no substantial potential drop occurs inside the nanopores. As a consequence,

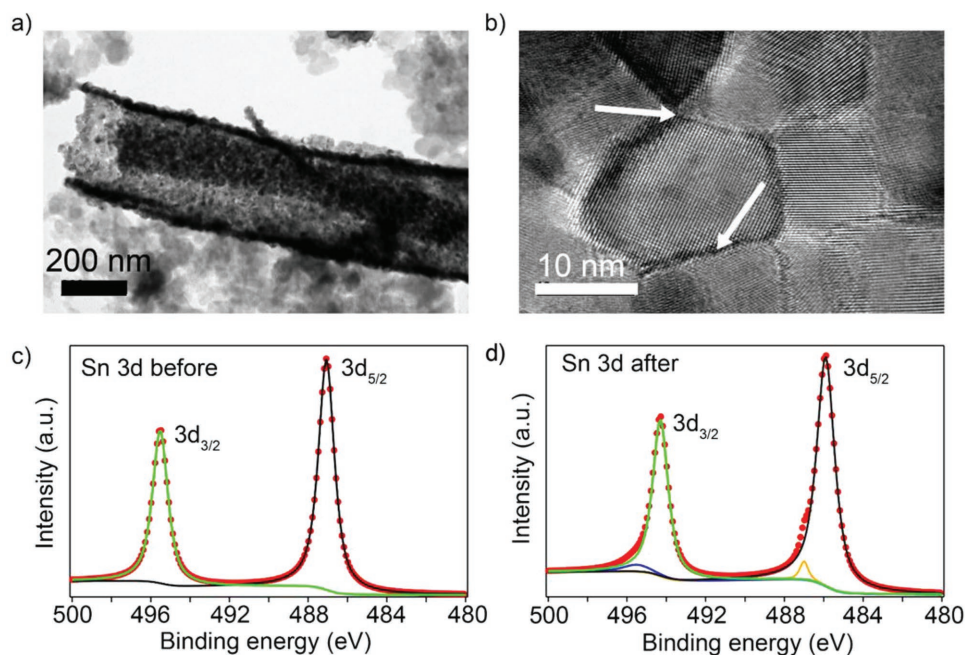


Figure 6. a,b) HRTEM image of the WIT SnO₂ after reduction. c,d) XPS results of the WIT SnO₂ electrode before (c) and after (d) electrolysis.

the inner surface of the WIT SnO₂ nanoporous structures is not accessible or active for ERC.^[38–40] The active surface area is much lower than the measured BET surface area. Thus high catalyst surface area alone cannot account for the observed electrocatalytic activity enhancement.

The catalyst activity correlates with not only surface areas but also many other factors, such as particle size, density of GBs, and applicable field-induced reagent concentration. All factors mentioned above are possibly resulted in the catalysis activity enhancement through improving the electronic and chemical properties. They are analyzed as following: (1) the average particle size of WIT SnO₂ is 10–20 nm (shown in Figure 2e), while the commercial SnO₂ nanoparticle has an average particle size of 70 nm (Figure S2, Supporting Information). As previously reported, the smaller the particle size, the better catalytic activity and the higher FEs are expected.^[41–43] Thus, it is the first reason that the WIT SnO₂ catalyst exhibited enhanced activity in this work. (2) Recent studies have suggested GBs within the nanopores could engender high activity for CO₂ reduction, via reforming the adsorbate–metal bonding strengths thus stabilize catalytically active surfaces. Moreover, the surface-area-normalized activity for CO₂ reduction is found to be linearly correlated with GB surface density on metal NPs.^[36,44] So we speculate the increased density of GBs and nanoporous morphology of the WIT SnO₂ is another reason account for the high catalytic activity. (3) Field-induced reagent concentration (FIRC) concept can also be employed to explain the catalysis activity enhancement. Sargent and co-workers^[45] reported that local higher electric fields concentrate cations on nanostructured rods compared to on nanoparticles, then a higher local concentration of CO₂ close to the active surface, consequently enhanced ERC. This FIRC effect is also applicable to our WIT nanostructure of the SnO₂ catalyst. The FIRC effect at the WIT nanostructure might help stabilize the

adsorbed *CO₂[–] intermediates leading to the superiority in the ERC.

3. Conclusion

The WIT SnO₂ nanofiber catalysis was synthesized for highly selective ERC to C₁ products. The nanostructure and morphology of the WIT SnO₂ nanofiber is confirmed by SEM and TEM. In the ERC catalytic activity evaluation, the WIT SnO₂ electrode shows higher current density and FE for the formation of C₁ products, i.e., HCOOH and CO, compared to the NP SnO₂. With the reduced WIT SnO₂ catalyst, the maximum FE for C₁ products is as high as 93%. This superior selectivity to C₁ products together with substantial suppression of the HER can be simultaneously achieved at a very wide potential range from –0.89 to –1.29 V. Meanwhile the overpotential for ERC is only about 400 mV for the WIT SnO₂ nanofiber. Besides the high activity, the WIT SnO₂ nanofiber also possesses good long-term stability. Detailed characterizations including HRTEM and BET were employed to reveal possible enhancement mechanisms. Large surface area, WIT nanostructure and microporous inner tube, high density of GBs as well as the FIRC effect are likely attributed to its excellent catalytic performance. The developed facile and cost-effective synthesis process, high current density and selectivity to C₁ products, lower overpotential, and great chemical stability make the novel reduced WIT SnO₂ nanofiber a promising catalyst for ERC.

4. Experimental Section

Chemicals: Tin chloride dehydrate (SnCl₂·2H₂O, 99.99%, Aladdin), PVP (*M_w* = 1 300 000, Alfa Aesar), DMF (99.5%, Macklin), ethanol

(AR, Sinopharm Chemical Reagent Co. Ltd), potassium bicarbonate (KHCO₃, ≥99.99%, Sigma-Aldrich), Nafion solution (5 wt%, Sigma-Aldrich), and carbon dioxide (CO₂, 99.995%, Specialty Gases Co. Ltd) were used as received. Deionized water (18.2 MΩ, Milli-Q water purification system) was used to prepare electrolyte solutions. SnO₂ nanoparticle (99.99%, 50–70 nm, Macklin) and carbon paper (Hesen Co. Ltd, HPCP030) were used in control experiments.

Catalysts Synthesis and Electrode Preparation: The WIT SnO₂ nanofiber was fabricated by electrospinning. Briefly, 1.5 g SnCl₂·2H₂O and 1.0 g PVP were dissolved in 10 mL mixed solvents (DMF with ethanol, 1:1 by volume) with magnetic stirring for 12 h at room temperature. Obtained solution was used as the precursor for electrospinning. Carbon paper was used to collect the pristine nanofibers. The voltage was set at 15 kV, the distance between the carbon paper and the needle was 15 cm, and the precursor flow rate was 40 μL min⁻¹. The obtained electrospun nanofibers were then oxidized at 500 °C for 2 h at atmosphere. The NP SnO₂ was commercially available and used as received.

The catalysts loaded electrodes were prepared using a drop-casting deposition method. Carbon paper was used as the electrode substrate after cleaning with acetone and deionized water. WIT SnO₂ nanofibers and NP SnO₂ inks for drop-casting deposition were prepared by mixing carbon black (CB, 10 mg), WIT SnO₂ nanofibers or NP SnO₂ (10 mg), Nafion solution (0.5 wt%, 100 μL), and alcohol (1 mL). The mixture was then sonicated for 60 min after high speed stirring overnight and drop-casted (≈100 μL) onto the carbon paper (1 × 1 cm²). The catalyst loading was ≈1 mg cm⁻². Then, the electrodes were dried at 60 °C for 2 h. Carbon black was chosen as the support and dispersing agent due to its high conductivity and stability.^[46]

Material Characterization: The morphology of the WIT SnO₂ nanofibers and NP SnO₂ was observed by SEM (SU-8010, Hitachi) and TEM (200 KV-2100F, JEOL). XRD (Shimadzu) was used to determine the crystalline structure of the WIT SnO₂ nanofibers and NP SnO₂. Automatic surface area and porosity analyzer (Micromeritics) was employed to record the nitrogen adsorption–desorption isotherms. The specific surface area and pore size distributions were estimated by BET and Barrett–Joyner–Halenda methods, respectively. Surface elemental analysis of the WIT SnO₂ nanofiber before and after electrochemical reaction was conducted on Escalab 250Xi (Thermo Fisher Scientific) XPS with an Mg Kα X-ray resource.

Electrochemical CO₂ Reduction Activity Evaluation: Electrochemical CO₂ reduction was performed in a gastight two-compartment electrochemical cell separated by a Nafion 117 membrane with a three-electrode setup (schematic diagram shown as Figure S1, Supporting Information). A Biologic VP-300 electrochemical workstation was used to precisely control the working electrode potential in chronoamperometry mode using a Pt mesh counter electrode and an Ag/AgCl reference electrode (3.0 M KCl, 0.210 V vs SHE). The reference electrode potentials were converted to RHE using the formula below

$$E(\text{RHE}) = E(\text{Ag/AgCl}) + 0.210 \text{ V} + 0.0591 \text{ V} \times \text{pH} \quad (1)$$

All potentials present in this paper were versus RHE, unless stated otherwise. The electrolyte solution in both compartments was 0.1 M KHCO₃ (pH = 6.8, after purging CO₂ for 1 h). CO₂ was continuously purged into the cathodic compartment (20 mL min⁻¹) through a gas diffuser during the constant potential electrolysis. All electrocatalytic tests were carried out at a constant temperature of 25 °C.

CO₂ Reduction Products Quantification: A gas chromatograph (GC, 9790, Fuli Co. Ltd) with a thermal conductivity detector and a flame ionization detector was used to quantify the concentration of gaseous products including H₂ and CO. Products concentration measured by the GC were averaged across aliquots. H₂ and CO production rate and FE were determined based on their concentrations as reported previously.^[47] Liquid products of the electrochemical reduction of CO₂ were quantified using 1D ¹H NMR. ¹H spectra were recorded on Bruker Avance DRX 400 (500 MHz). The water peak was suppressed by a modified WET solvent suppression technique. 600 μL of the electrolyte after electrolysis containing CO₂ reduction products was mixed with 70 μL of 10 × 10⁻³ M

dimethylsulfoxide as internal standard in D₂O for NMR analysis. The same acquisition parameters were chosen for all NMR spectra, notably a minimum of 64 scans for a clearer distinction between signal and noise.

Supporting Information

Supporting Information is available from the Wiley Online Library or from the author.

Acknowledgements

L.F. and Z.X. contributed equally to this work. The authors acknowledge the financial support from the National Key R&D Program of China (2016YFA0202900), the Natural Science Foundation of China (Grant Nos. 21436007, 21576235, U1462201, and 21676242) and the Zhejiang Provincial Natural Science Foundation (Grant No. LY16B060005). L.F. thanks Prof. Qiaohong He, Prof. Xiaokun Ding, and Prof. Fang Chen of the Department of Chemistry, Zhejiang University for TEM and SEM analyses. Z.X. thanks Jianyang Pan (Pharmaceutical Informatics Institute, Zhejiang University) for performing NMR spectrometry for structure elucidation.

Conflict of Interest

The authors declare no conflict of interest.

Keywords

C₁ products, CO₂ reduction, grain boundaries, 1D SnO₂, wire-in-tube structures

Received: October 30, 2017

Revised: January 20, 2018

Published online:

- [1] W. Wang, S. Wang, X. Ma, J. Gong, *Chem. Soc. Rev.* **2011**, *40*, 3703.
- [2] J. Qiao, Y. Liu, F. Hong, J. Zhang, *Chem. Soc. Rev.* **2014**, *43*, 631.
- [3] M. Alvarez-Guerra, J. Albo, E. Alvarez-Guerra, A. Irbien, *Energy Environ. Sci.* **2015**, *8*, 2574.
- [4] X. Duan, J. Xu, Z. Wei, J. Ma, S. Guo, S. Wang, H. Liu, S. Dou, *Adv. Mater.* **2017**, *29*, 1701784.
- [5] H. Mistry, A. S. Varela, S. Kühl, P. Strasser, B. R. Cuenya, *Nat. Rev. Mater.* **2016**, *1*, 16009.
- [6] Y. Li, Q. Sun, *Adv. Energy Mater.* **2016**, *6*, 1600463.
- [7] F. Li, L. Chen, G. P. Knowles, D. R. MacFarlane, J. Zhang, *Angew. Chem., Int. Ed.* **2017**, *56*, 505.
- [8] H. Uslu, C. Bayat, S. Goekmen, Y. Yorulmaz, *J. Chem. Eng. Data* **2009**, *54*, 48.
- [9] Y. Wang, J. Zhou, W. Lv, H. Fang, W. Wang, *Appl. Surf. Sci.* **2016**, *362*, 394.
- [10] C. Delacourt, P. L. Ridgway, J. B. Kerr, J. Newman, *J. Electrochem. Soc.* **2008**, *155*, B42.
- [11] W. Zhu, Y. J. Zhang, H. Zhang, H. Lv, Q. Li, R. Michalsky, A. A. Peterson, S. Sun, *J. Am. Chem. Soc.* **2014**, *136*, 16132.
- [12] Q. Lu, J. Rosen, Y. Zhou, G. S. Hutchings, Y. C. Kimmel, J. G. Chen, F. Jiao, *Nat. Commun.* **2014**, *5*, 3242.
- [13] Y. Chen, C. W. Li, M. W. Kanan, *J. Am. Chem. Soc.* **2012**, *134*, 19969.
- [14] M. B. Ross, C. T. Dinh, Y. Li, D. Kim, P. De Luna, E. H. Sargent, P. Yang, *J. Am. Chem. Soc.* **2017**, *139*, 9359.

- [15] L. Zhang, Z. J. Zhao, J. Gong, *Angew. Chem., Int. Ed.* **2017**, *56*, 11326.
- [16] D. D. Zhu, J. L. Liu, S. Z. Qiao, *Adv. Mater.* **2016**, *28*, 3423.
- [17] Z. Xia, M. Freeman, D. Zhang, B. Yang, L. Lei, Z. Li, Y. Hou, *ChemElectroChem* **2018**, *5*, 211.
- [18] S. Gao, X. Jiao, Z. Sun, W. Zhang, Y. Sun, C. Wang, Q. Hu, X. Zu, F. Yang, S. Yang, L. Liang, J. Wu, Y. Xie, *Angew. Chem., Int. Ed.* **2016**, *55*, 698.
- [19] J. Qu, X. Zhang, Y. Wang, C. Xie, *Electrochim. Acta* **2005**, *50*, 3576.
- [20] Y. Chen, M. W. Kanan, *J. Am. Chem. Soc.* **2012**, *134*, 1986.
- [21] Y. Zhao, J. Liang, C. Wang, J. Ma, G. G. Wallace, *Adv. Energy Mater.* **2018**, <https://doi.org/10.1002/aenm.201702524>.
- [22] F. Li, S.-F. Zhao, L. Chen, A. Khan, D. R. MacFarlane, J. Zhang, *Energy Environ. Sci.* **2016**, *9*, 216.
- [23] X. Duan, J. Xu, Z. Wei, J. Ma, S. Guo, H. Liu, S. Dou, *Small Methods* **2017**, *1*, 1700156.
- [24] F. Li, L. Chen, M. Xue, T. Williams, Y. Zhang, D. R. MacFarlane, J. Zhang, *Nano Energy* **2017**, *31*, 270.
- [25] B. Kumar, M. Asadi, D. Pisasale, S. Sinha-Ray, B. A. Rosen, R. Haasch, J. Abiade, A. L. Yarin, A. Salehi-Khojin, *Nat. Commun.* **2013**, *4*, 2819.
- [26] S. Zhang, P. Kang, S. Ubnoske, M. K. Brennaman, N. Song, R. L. House, J. T. Glass, T. J. Meyer, *J. Am. Chem. Soc.* **2014**, *136*, 7845.
- [27] B. Kumar, V. Atla, J. P. Brian, S. Kumari, T. Q. Nguyen, M. Sunkara, J. M. Spurgeon, *Angew. Chem., Int. Ed.* **2017**, *56*, 3645.
- [28] L. Fan, W. Zhang, S. Zhu, Y. Lu, *Ind. Eng. Chem. Res.* **2017**, *56*, 2046.
- [29] Q. Wei, F. Xiong, S. Tan, L. Huang, E. H. Lan, B. Dunn, L. Mai, *Adv. Mater.* **2017**, *29*, 1602300.
- [30] Z. Fan, H. Zhang, *Acc. Chem. Res.* **2016**, *49*, 2841.
- [31] K. R. Yoon, G. Y. Lee, J. W. Jung, N. H. Kim, S. O. Kim, I. D. Kim, *Nano Lett.* **2016**, *16*, 2076.
- [32] J. J. Wu, D. W. Zeng, X. X. Wang, L. Zeng, Q. W. Huang, G. Tang, C. S. Xie, *Langmuir* **2014**, *30*, 11183.
- [33] S. J. Peng, L. L. Li, Y. X. Hu, M. Srinivasan, F. Y. Cheng, J. Chen, S. Ramakrishna, *ACS Nano* **2015**, *9*, 1945.
- [34] C. W. Li, J. Ciston, M. W. Kanan, *Nature* **2014**, *508*, 504.
- [35] X. Feng, K. Jiang, S. Fan, M. W. Kanan, *J. Am. Chem. Soc.* **2015**, *137*, 4606.
- [36] K.-S. Kim, W. J. Kim, H.-K. Lim, E. K. Lee, H. Kim, *ACS Catal.* **2016**, *6*, 4443.
- [37] M. F. Baruch, J. E. Pander III, J. L. White, A. B. Bocarsly, *ACS Catal.* **2015**, *5*, 3148.
- [38] S. Sen, D. Liu, G. T. R. Palmore, *ACS Catal.* **2014**, *4*, 3091.
- [39] H. Boo, S. Park, B. Ku, Y. Kim, J. H. Park, H. C. Kim, T. D. Chung, *J. Am. Chem. Soc.* **2004**, *126*, 4524.
- [40] J. H. Bae, J.-H. Han, T. D. Chung, *Phys. Chem. Chem. Phys.* **2012**, *14*, 448.
- [41] D. Gao, H. Zhou, J. Wang, S. Miao, F. Yang, G. Wang, J. Wang, X. Bao, *J. Am. Chem. Soc.* **2015**, *137*, 4288.
- [42] R. Reske, H. Mistry, F. Behafarid, B. Roldan Cuenya, P. Strasser, *J. Am. Chem. Soc.* **2014**, *136*, 6978.
- [43] S. Zhang, P. Kang, T. J. Meyer, *J. Am. Chem. Soc.* **2014**, *136*, 1734.
- [44] X. Feng, K. Jiang, S. Fan, M. W. Kanan, *ACS Cent. Sci.* **2016**, *2*, 169.
- [45] M. Liu, Y. Pang, B. Zhang, P. De Luna, O. Voznyy, J. Xu, X. Zheng, C. T. Dinh, F. Fan, C. Cao, F. P. de Arquer, T. S. Safaei, A. Mepham, A. Klinkova, E. Kumacheva, T. Filleter, D. Sinton, S. O. Kelley, E. H. Sargent, *Nature* **2016**, *537*, 382.
- [46] O. A. Baturina, Q. Lu, M. A. Padilla, L. Xin, W. Li, A. Serov, K. Artyushkova, P. Atanassov, F. Xu, A. Epshteyn, T. Brintlinger, M. Schuette, G. E. Collins, *ACS Catal.* **2014**, *4*, 3682.
- [47] D. Ren, Y. Deng, A. D. Handoko, C. S. Chen, S. Malkhandi, B. S. Yeo, *ACS Catal.* **2015**, *5*, 2814.